Bollettino della Società Paleontologica Italiana, 63 (3), 2024, 229-244. Modena

Microbe-mineral interactions in the microstromatolitic crusts of the lacustrine chimneys and volcanic bedrock of Lake Abhe, Republic of Djibouti

Victor A.C. Dorneles, Keyron Hickman-Lewis, Roberto Barbieri, Antoine M. Caminiti & Barbara Cavalazzi*

V.A.C. Dorneles, Dipartimento di Scienze Biologiche, Geologiche e Ambientali - BiGeA, Università di Bologna, Via Zamboni 67, I-40126 Bologna, Italy; victoramir.cardoso2@unibo.it
K. Hickman-Lewis, School of Natural Sciences, Birkbeck, University of London, Malet Street London WC1E 7HX, United Kingdom; Department of Earth Science and Engineering, Imperial College London, London, United Kingdom; k.hickman-lewis@bbk.ac.uk
R. Barbieri, Dipartimento di Scienze Biologiche, Geologiche e Ambientali - BiGeA, Università di Bologna, Via Zamboni 67, I-40126 Bologna, Italy; roberto.barbieri@unibo.it
A.M. Caminiti, Centre d'Étude et de Recherche de Djibouti - CERD Djibouti, H583+MH3, Djibouti, Republic of Djibouti; antoinecaminiti@yahoo.fr
B. Cavalazzi, Dipartimento di Scienze Biologiche, Geologiche e Ambientali - BiGeA, Università di Bologna, Via Zamboni 67, I-40126 Bologna, Italy; Department of Geology, University of Johannesburg, Auckland Park 2006, South Africa; barbara.cavalazzi@unibo.it *corresponding author*

KEY WORDS - Microbial crust, cyanobacteria, preservation potential, hyperalkaline lake, East African Rift System.

ABSTRACT - Utilising a multi-analytical approach, we investigated centimetre-scale domical and tabular microstromatolitic encrustations from Lake Abhe, a hyperalkaline and hypersaline environment in the Afar Rift, Djibouti. We explored the complex interactions between microorganisms and sediments, alongside the preservation potential of microfossils in this extreme setting. Using optical and scanning electron microscopy, we found that the microstromatolitic crusts exhibit both abiogenic and biogenic characteristics and fabrics, influenced by the mixing of lacustrine and hydrothermal fluids and microbial activity. Microcolumnar fabrics, composed of micrite and microsparite laminae, likely formed in calm, supersaturated water conditions and were mediated by microbial mineralisation. Crystalline fabrics, on the other hand, appear to originate from inorganic processes, followed by early diagenetic growth of larger crystals of Mg-calcite. Filamentous cyanobacterial sheaths, preserved within the crusts and often perpendicular to laminations, suggest a photosynthetic growth mode. Extracellular polymeric substances played a key role in microbial carbonate formation by providing nucleation sites for mineral precipitation and anchoring microbes to their substrates. Raman microspectroscopy reveals a concentration of carbonaceous materials within the carbonate matrix; these are closely associated with filamentous sheaths, suggesting their biological origin. The preservation of these biogenic components is also linked to the presence of Mg-bearing silicates, which are likely tied to microbial activity and high pH conditions, consistent with observations in other alkaline lacustrine systems. This study offers insights into microbial carbonate formation and biosignature preservation in extreme alkaline environments, contributing to our understanding of early Earth microbial ecosystems.

INTRODUCTION

Stromatolites are organo-sedimentary structures that reflect complex interactions between microbial consortia and their sedimentary environments (Burne & Moore, 1987; Bosak et al., 2013). The fossil record of stromatolites provides an intriguing microbial archive, extending at least to the Palaeoarchaean (e.g., Hickman-Lewis et al., 2023) and their architect microbes may have retained similar ecological functions and characteristics since that time (Bosak et al., 2013). Although widespread throughout the Archaean and Proterozoic, stromatolites are now restricted to extreme environments, to which they are particularly resilient (Riding, 2011; Noffke & Awramik, 2013; Coman et al., 2015). Although living stromatolites are perhaps best-known from (shallow) marine environment such as Hamelin Pool, Shark Bay, Western Australia (e.g., Papineau et al., 2005; Jahnert & Collins, 2012), and Highborne Cay, the Bahamas (e.g., Foster et al., 2009; Nutman et al., 2016), living stromatolites have also been reported in a multitude of lacustrine extreme environments including Lake Van, the world's largest alkaline lake, in eastern Turkey (Çağatay et al., 2024), the high-altitude volcanic Lake Socompa in the Argentinean Andes, South America (Farías et al., 2013), and the hydrothermally influenced Lake Bogoria (McCall, 2010) and Lake Turkana (Zăinescu et al., 2023) in the East African Rift System in Kenya. Investigating stromatolite formation and preservation within such settings may provide insights into the development of such ecosystems in deep time.

The Afar Depression and the East African Rift system, characterised by zones of thinned continental lithosphere related to asthenospheric intrusions from the upper mantle, graben valleys and basins, major faults, seismicity and volcanism (e.g., Corti, 2009; Cavalazzi et al., 2019), features a large number of hydrothermally influenced pools and lakes, hot and warm springs that host a large variety of polyextreme environments and relatively poorly studied stromatolite-forming microbial consortia (e.g., Casanova, 1994; McCall, 2010).

Lake Abhe (11°11'50.66"N/41°46'50.91"E), also spelled Abbe or Abbé, is located on the southern-western edge of the Republic of Djibouti across its border with Ethiopia (Fig. 1). Lake Abhe is part of the eastern branch of the East African Rift system and is well-known for its large carbonate chimneys (Fontes & Pouchan, 1975; Caminiti, 2000; Dekov et al., 2014, 2021; Le Gall et al.,

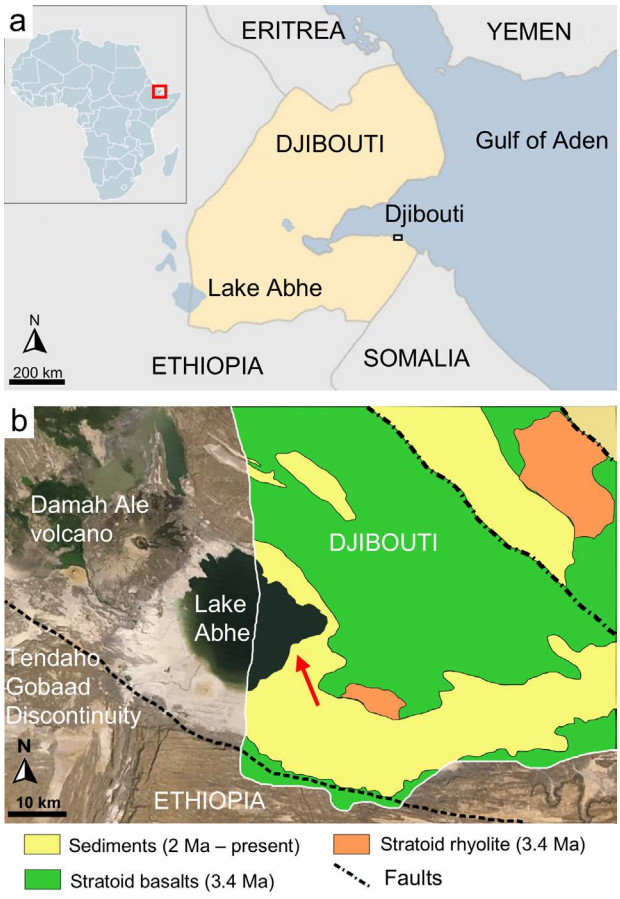

Fig. 1 - Location of the study area. a) Simplified map showing the location of Lake Abhe. b) Simplified geological map of Lake Abhe and its surrounding (adapted from Boschetti et al., 2018), showing the location of chimneys (arrowed) on the south-eastern margin of the lake (geology of Djibouti shown). Data source: Google Earth (2024 imagery: CNES/Airbus-Landsat; 2034 imagery: DigitalGlobe).

2018; DeMott et al., 2021). These chimneys formed on the floor of the hypersaline, hyperalkaline, hydrothermally influenced lake and are now exposed near the south-eastern coast of the lake (Figs 1-2); together with basaltic rocks outcropping in the area, these chimneys exhibit peculiar microstromatolitic crusts (Dekov et al., 2014, 2021; Le Gall et al., 2018; DeMott et al., 2021).

Here, we present a detailed study of the carbonate fabrics of peculiar microstromatolitic encrustations from lacustrine chimneys and volcanic bedrocks of Lake Abhe. We used a multi-analytical approach, seeking to understand the relationship between microorganisms and encrustations, and the preservation potential of microfossils in this hyperalkaline and hypersaline polyextreme lake.

GEOLOGICAL SETTING

Lake Abhe is located within the Afar Rift, a depression formed by the intersection of the Main Ethiopian Rift with the oceanic Gulf of Aden and Red Sea Rifts (e.g., Tesfaye et al., 2003; Corti, 2009; Varet, 2018). The Afar region is a wide, complex and tectonically active area dominated by predominantly NW-SE oriented tensional faulting, creating a horst-graben system hosting residual lakes (Tesfaye et al., 2003). Lake Abhe is located in the western section of the Gobaad tectonic basin, an E-W-striking system linked to the larger Tendaho Rift system, which developed during the Pleistocene-Holocene on a volcanic basement mainly composed of basalts and subordinate acid rocks (Fig. 1b) (Abbate et al., 1995; Tesfaye et al., 2003; Varet, 2018). The oldest exposed sedimentary rocks in the Gobaad basin are the Early Pleistocene lacustrine shales interstratified within Stratoid Series basaltic lava flows, diatomites, gypsum and ash flows (Gasse & Street, 1978), followed by Lower and Middle Holocene carbonate-dominated deposits of lakes including stromatolitic crusts, littoral deposits with ripple marks and shell accumulations (e.g., Gasse & Street, 1978).

Lake Abhe and carbonate chimneys

Lake Abhe (Fig. 1), located ESE of the Damah Ale volcano, is an hyperalkaline (pH = 9.9-10) and hypersaline (TDS > 90,000 mg) lake at 240 m above sea level, with an area larger than 350 km^2 and an average depth of 12-15 m (Valette, 1975; Caminiti, 2000; Dekov et al., 2014, 2021; Awaleh et al., 2015). Lake Abhe is fed by the Awash River, a major river of the Ethiopian Plateau. A wide, flat area (up to 5 km^2) surrounding the eastern shoreline of the Lake Abhe is typified by lacustrine deposits and isolated and/or coalescent carbonate chimneys, reaching heights of up to 35 m (Fontes & Pouchan, 1975; Dekov et al., 2014; Le Gall et al., 2018; DeMott et al., 2021; Walter et al., 2023; Fig. 2).

The Lake Abhe chimneys formed due to carbonate precipitation from the mixing of sulphide-calcium hydrothermal fluids and carbonate-soda lake waters (Caminiti, 2000; Dekov et al., 2014, 2021), consistent with the high pH and salinity increases caused by changes in the course of the Awash River and the arid climate of Afar (Awaleh et al., 2015; DeMott et al., 2021). Hot springs at the bottom of the chimneys discharge effluent with pH 7-9 and temperatures of 90-100 °C (Caminiti, 2000). Isotopic data of ^{13}C and ^{18}O ($\delta^{18}O$ = -2.25‰ and $\delta^{13}C$ = +0.67‰, Fontes & Pouchan, 1975) in the Afar Rift, indicate a

Fig. 2 - Relict hydrothermal carbonate chimneys at the south-eastern shore (see Fig. 1) of Lake Abhe, Republic of Djibouti. a) Isolated chimneys. b) Chain of coalescing chimneys.

dominant influence from highland runoff with a minor contribution from evaporation (Gasse & Street, 1978; Gasse & Fontes, 1989). Awaleh et al. (2015) suggested that the Lake Abhe geothermal reservoir is recharged by meteoric water infiltrating the regional aquifer and descending through volcanic fractures, mixing with fluids undergoing deep regional circulation, which causes the water to heat, ascend and discharge through hot springs. The formation of carbonate chimneys is also associated with fluctuations in the level of Lake Abhe as recorded in its lacustrine carbonate deposits (e.g., Fontes & Pouchan, 1975; Gasse & Street, 1978; Gutherz et al., 2015; Gasse, 2000), characterised by major episodes of aridity during the Late Pleistocene, followed by transgressive events throughout the Holocene (between 8000 and 6000 years before present), when the lake experienced high-water levels, then a decrease in lake level (between 6300 to 2700 years before present), corresponding to alternating dry and wet climatic phases.

MATERIALS AND METHODS

The microstromatolitic crusts studied herein were collected in 2018 during a field campaign at Lake Abhe. The sampled outcrops are located on the south-eastern shores of the lake (see Fig. 1) and include microstromatolites encrusting carbonate chimneys and basaltic bedrock (Fig. 3). Microstromatolitic crusts reach thicknesses of up to 25 cm, exhibit distinct internal layering and external patterns, and occur in direct contact with the underlying carbonate and volcanic substrate (Figs 3-4).

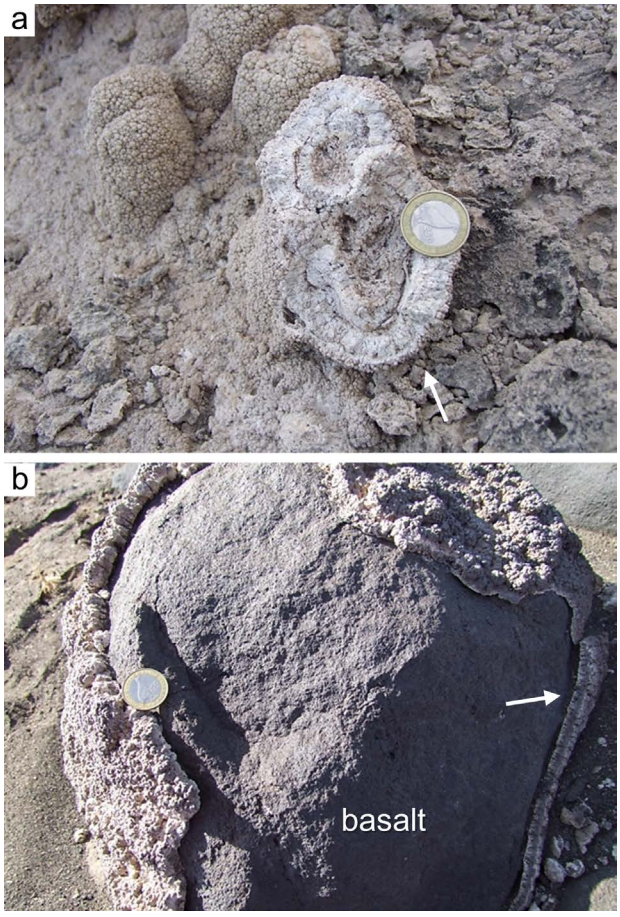

Fig. 3 - Outcrop photographs of microstromatolitic crusts (arrows) growing on different bedrock types from the south-eastern shores of Lake Abhe. a) Representative stromatolitic crust formed on the exterior of a carbonate chimney. b) Representative stromatolitic crust developed directly on basaltic bedrock. Coin (29 mm in diameter) for scale.

Sample preparation and analyses were performed at the Dipartimento di Scienze Biologiche, Geologiche e Ambientali, Università di Bologna, Italy. Samples were embedded in epoxy resin to produce standard petrographic thin sections (~40 μm thick), which were used for optical microscopy and Raman microspectroscopy. Microfabric descriptions were performed via thin section analysis using a ZEISS Axiophot optical microscope equipped with a Nikon DS-Fi2 digital camera. These observations were complemented by Raman microspectroscopy performed using an Oxford WITec Alpha300 R microscope equipped with a 532 nm green laser. Raman spectra were collected using a 100× Nikon objective and a frequency doubled Nd:YAG (532 nm) Ar-ion 20 mW monochromatic laser source. Beam centring and spectral calibration were performed before spectral acquisition using a Si standard (111) with a characteristic Si Raman peak at 520.4 cm^{-1}, whereas the optimum power for the analyses of different mineral phases was determined experimentally. Raman analyses were visualised and interpreted using WITec Project Management and Image Project Plus software suite and compared with reference spectra from the RRUFF database (Laetsch & Downs, 2006), Frezzotti et al. (2011) and Cavalazzi et al. (2012). Scanning electron microscopy and energy dispersive X-ray spectroscopy (SEM-EDX) analyses were performed using a JEOL JSM-5400 scanning electron microscope equipped with an iXRF Si-drift EDX detector with an ultra-thin window, operating at 15 kV. Observations were performed on gold-coated, freshly fractured fragments of samples.

RESULTS

Microstromatolitic crusts occur as centimetre-scale domical and tabular structures with layered internal fabrics and a popcorn-like (sensu DeMott et al., 2021) external texture (Fig. 4a-c).

Stromatolitic domical crusts are composed of several centimetre-scale layers enveloping a friable and porous (sugary texture sensu DeMott et al., 2021) calcitic core (Fig. 4a, d). The internal domical crusts show layers with distinct fabrics: microcolumnar, crystalline and coated grains (Fig. 4). The most common is the microcolumnar fabric, which often occurs immediately surrounding the calcitic core (Fig. 4a). This is followed by the crystalline fabric, which generates the external popcorn-like texture (Fig. 4c). Rarely, the calcitic core is directly covered by crystalline and/or rounded carbonate-coated grains, up to 2 mm in diameter (Fig. 4d).

Tabular microstromatolitic crusts are also characterised by microcolumnar, crystalline and coated grain fabrics (Fig. 4b) which mostly occur as a flat to slightly wavy laminated structure dominated by microcolumnar fabrics growing directly on the basaltic bedrock and overlain by a layer of crystalline fabric.

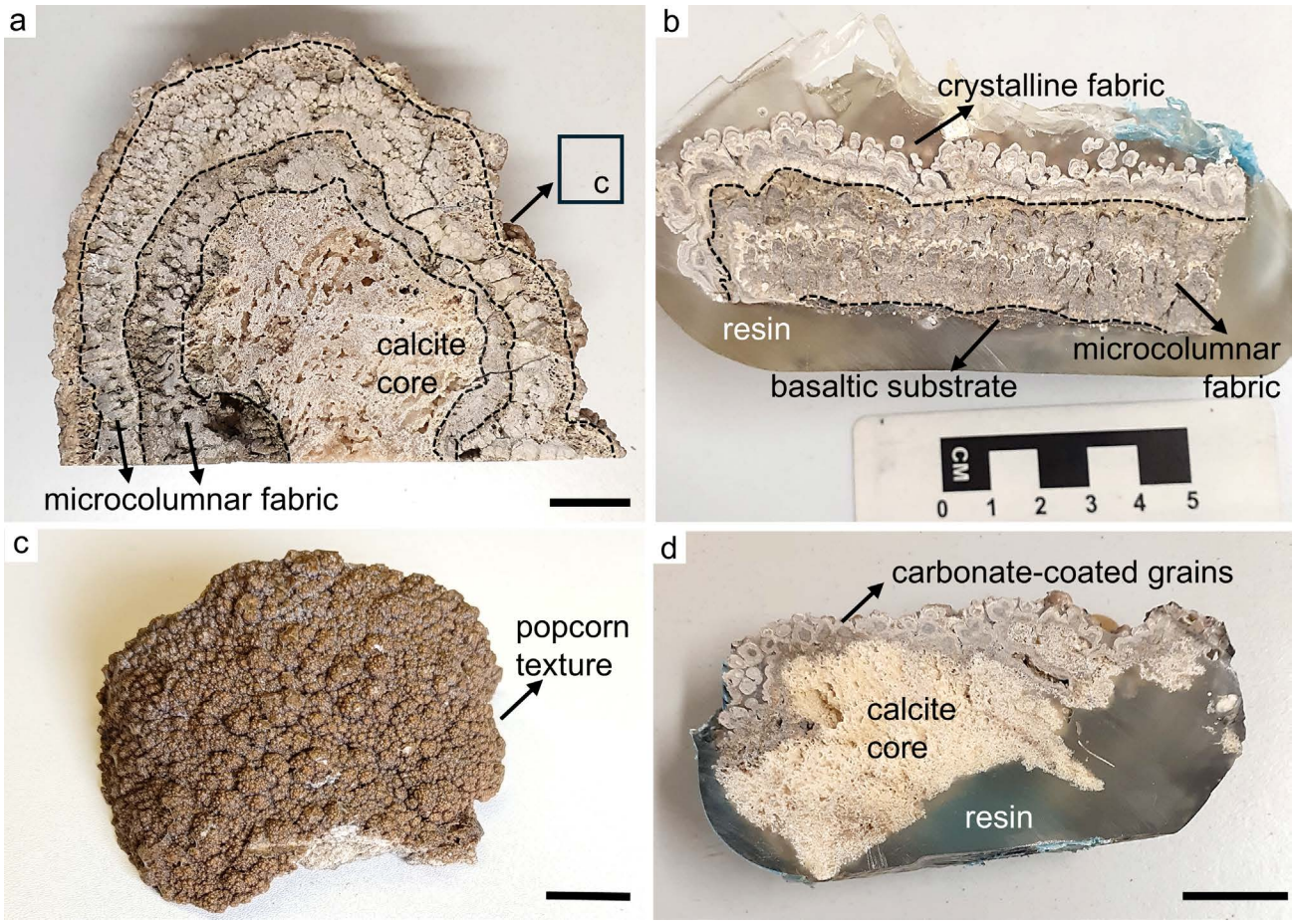

Fig. 4 - Hand samples of microstromatolitic crusts; all samples are oriented as collected. a) Stromatolitic dome formed of a calcite core enveloped by layers of microcolumnar fabric. b) Fine laminations within the tabular stromatolite are formed of microcolumnar fabric at the bottom, and crystalline fabric at the top. Note the contact with basalt (bottom). c) Top view of the external crust of the domical sample in (a) exhibiting an external popcorn-like texture. d) Crust of coated grains covering a layer of crystalline fabric enveloping a calcite core. Scale bars equal 2 cm.

The transition between the different fabrics of the microstromatolitic crusts was also observed using optical microscopy. At the micro-scale, the transition is commonly marked by an erosional and/or sharp contact (Fig. 5), with no preference observed for the growth of one fabric over another.

Optical microscopy imaging shows that the domical and tabular microstromatolitic crusts are composed of microcolumnar, crystalline and coated grain fabrics, each of which exhibits distinctive characteristics. The microcolumns occur as closely packed, straight to slightly branched structures growing directly on the calcitic core (Fig. 6a). Less than 1 mm high and 0.1 to 0.6 mm wide, microcolumns consist of moderately to parabolic hemispherical convex ascending laminae. These laminae are laterally continuous and composed of thinner interlayers of brown micrite, characterised by a cryptocrystalline texture (grains < 4 μm), interspersed with thicker laminae composed of non-isopachous grey microsparite, characterised by a fine-grained calcite matrix (5-30 μm grains) (Fig. 6a). Locally, laterally linked microcolumnar layers with a maximum height of 0.7 mm (Fig. 6b). The calcitic core, on top of which microcolumn growth occurs, consists of highly porous (subhedral to euhedral) rhombohedral calcite crystals arranged in a translucent dendritic structure (Fig. 6c). The crystallin fabric is entirely composed of crystalline sparite calcite, featuring an internal flat lamination (Fig. 6d). The popcorn-like texture corresponds to the outermost part of the microstructures. Locally, rounded coated-carbonate grains (Fig. 6e) composed of autochthonous spherical fragments of crystalline calcite and coated by concentric sparite form sub-spherical to spherical pisoid-like structures (Fig. 6f).

Microsparite and micrite laminae forming the microcolumns host slightly curved, non-septate filamentous structures (Fig. 7) that occur as isolated filaments, commonly preserved in contact with wavy micritic laminae containing high concentrations of carbonaceous materials (CM; Fig. 7a-b). Some filamentous structures form clusters perpendicularly oriented relative to laminae growth, within both the micrite (Fig. 7c-d) and microsparite laminae (Fig. 7e); or as densely packed clusters exhibiting a palisade-like texture (Fig. 7f).

Using Raman microspectroscopy (Figs 8-9), filamentous structures are shown to be spatially associated with concentrations of CM and are embedded within a magnesian calcite matrix (identified by Raman bands at 155, 281, 713 and 1086 cm^{-1}; Fig. 8c, e). The CM in filamentous structures is characterised by bands of the

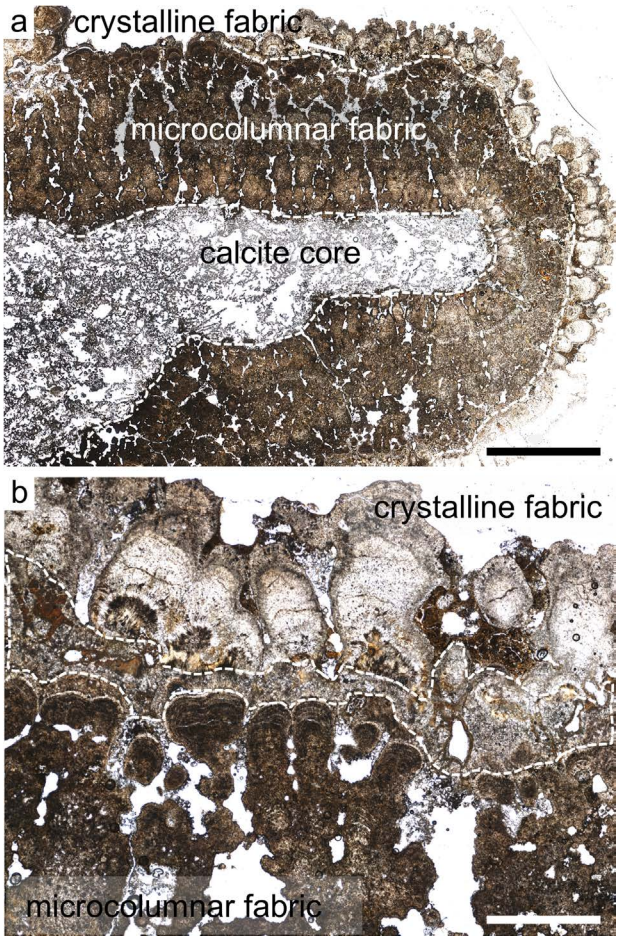

Fig. 5 - Optical photomicrographs showing transitions between the different fabrics of the microstromatolitic crusts. a) Microcolumnar fabric growing on top of the calcite core (note the sharp contact), also showing the overlying crystalline fabric. Scale bar equals 5 mm. b) Transition from microcolumnar to crystalline fabric showing erosional contacts (white dashed lines). Scale bar equals 1 mm.

first- (disordered carbon, D, at 1341 cm^{-1} and graphite, G, at 1596 cm^{-1}) and second-order (between 2500 and 3200 cm^{-1}) regions of the spectrum (Fig. 8d, f).

Crystalline fabrics show flat laminations in which molds of filamentous structures are poorly preserved (Fig. 9a-c). Raman microspectroscopy enabled the recognition of two main components in thin section (Fig. 9d-h): Mg-calcite in the matrix identified by major bands at 155, 281, 713 and 1087 cm^{-1} (Fig. 9e, g) and CM, characterised by the first-order D (1336 cm^{-1}) and G (1583 cm^{-1}) bands, and second-order bands (Fig. 9f, h).

SEM observations showed well-defined laminations (Fig. 10a) confirming that microcolumns are generated by alternating micrite layers of microgranular micrite and densely packed microsparite layers, both made of a Mg-calcite mineral phase (Fig. 10a). The calcite forming the cores of the microstromatolitic crusts shows large, well developed rhombohedral crystals of Mg-calcite (Fig. 10b).

SEM imaging also revealed the presence of microbial components within the laminated structures. Carbon-rich amorphous structures associated with filamentous structures were locally observed, showing different modes of occurrences:

1. A mucus-like texture distributed throughout the matrix, in which trace Na, Si and Cl were identified in EDX spectra (Fig. 11a), suggesting the presence of NaCl.

2. Amorphous structures occurring in association with a microgranular texture, composed of an aggregate of nano- to micrometric spherical particles (Fig. 11b). EDX data for this microgranular texture exhibit a variety of elements in trace quantities, including Na, Al, Si, Cl and K. The combined signals of Al-K with Si-O suggest the presence of aluminous phyllosilicates.

3. Porous alveolar networks with empty cavities (Fig. 11c) containing possible Mg-bearing silicate phases and a very low Ca content.

SEM observations of microstromatolitic crusts enablesdetailed characterisation of the filamentous structures and their two modes of preservation (Fig. 12): 1) empty molds of filamentous structures with no preferential orientation (Fig. 12a), which are the most common type of preservation; and 2) filamentous molds completely or partially filled with amorphous materials (Fig. 12b) that, although less common, preserve densely arrangements of parallel vertically oriented filaments forming a palisade-like texture, as previously observed using optical microscopy (Fig. 7c-f). EDX analyses demonstrated that the amorphous material filling the filamentous mold structures is composed of Si, O and Mg, suggesting the presence of Mg-silicate phases forming the counterpart of filamentous structures (Fig. 12c).

DISCUSSION

Formation of Lake Abhe microstromatolitic crusts

The formation of microstromatolitic crusts at Lake Abhe has previously been linked to rapid carbonate precipitation due to interactions between hydrothermal fluids and lake waters (Dekov et al., 2014); however, the role of microbial communities in the formation of these crusts remains poorly constrained.

The microcolumns forming the crusts have a laminated structure of dark micritic and light sparite calcite laminae, resembling stromatolites found throughout the geological record (Grotzinger & Knoll, 1999; Riding, 2011). Cyanobacteria are considered the primary microorganisms responsible for the formation of modern stromatolites (e.g., Schopf, 2012; Nguyen et al., 2022), the internal lamination of which generally results from the rhythmic stratification of cyanobacteria-rich laminae (containing fossilised filaments and sheaths) and more porous laminae with lower concentrations of microbial components (Grotzinger & Knoll, 1999). Due to continuous calcite precipitation, cyanobacteria must migrate upward to maintain access to sufficient sunlight for photosynthesis. As a result, the older biomass dies and is entombed beneath subsequent layers of living cyanobacteria.

The formation of the microstromatolitic crusts occurred underwater and reflects the reaction between Ca-rich hydrothermal waters and the surficial lake waters sourced from the Awash River, which caused a precipitation of $CaCO_3$ (Demange et al., 1971; Fontes & Pouchan, 1975; Dekov et al., 2014, 2021; DeMott et al., 2021). The chimneys present an alignment suggesting

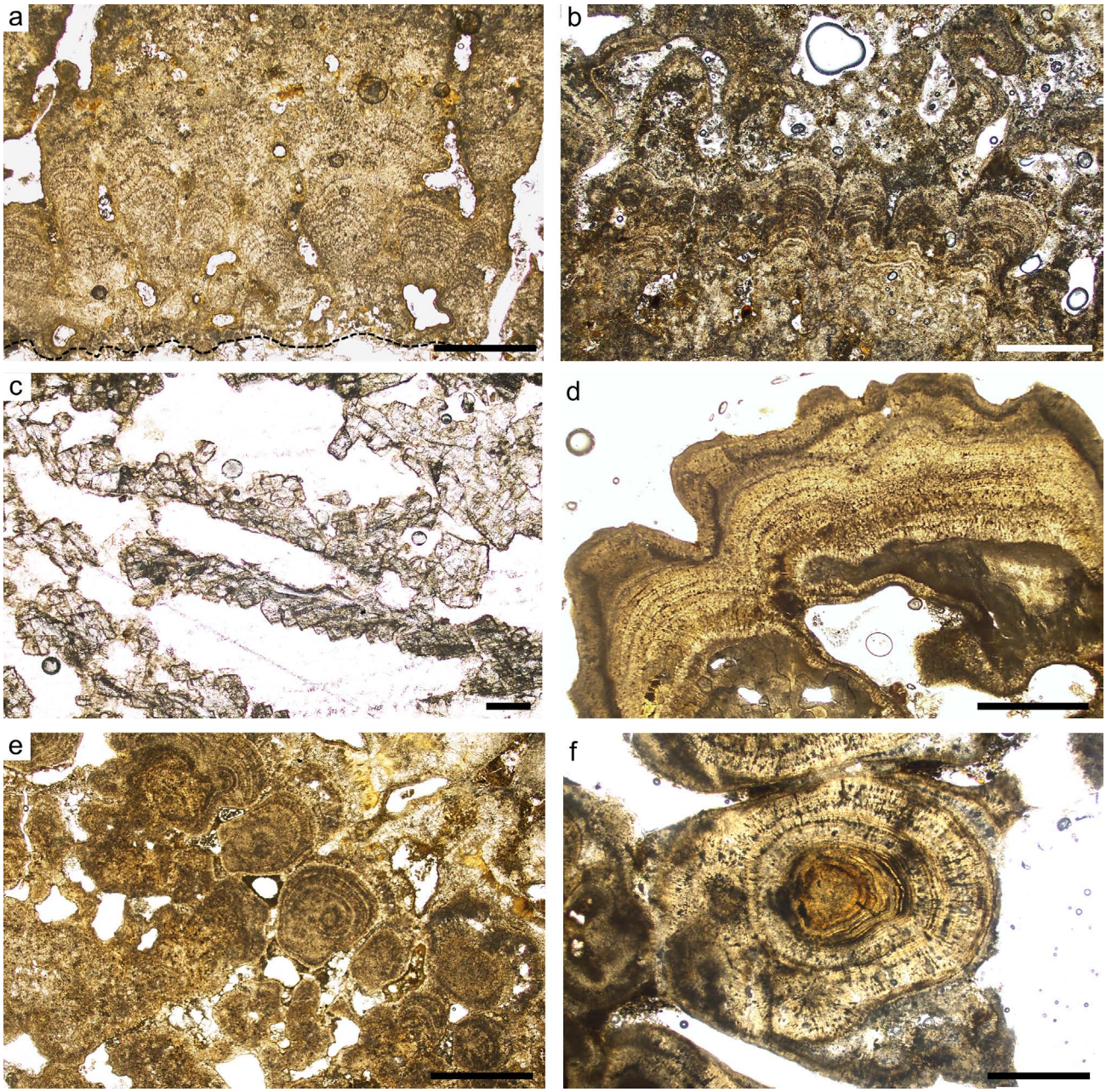

Fig. 6 - Optical photomicrographs showing representative fabrics of microstromatolitic crusts. a) Closely packed microcolumnar fabric. Scale bar equals 1 mm. b) Layered fabric composed of laterally linked microcolumns. Scale bar equals 1 mm. c) Calcitic core comprised of thin branches of translucent euhedral calcites. Scale bar equals 0.1 mm. d) Crystalline fabric showing internal lamination. Scale bar equals 1 mm. e) Packed carbonate-coated grains. Scale bar equals 1 mm. f) Representative spherical carbonate-coated grain with a core and concentric laminae resembling a pisoid-like structure. Scale bar equals 0.5 mm.

that they formed along active faults oriented WNW-ESE, which likely served as conduits for the percolation of fluids. Isotopic analyses (^{44}Ca, ^{13}C and ^{18}O) have revealed that the inner microstromatolitic crusts of the chimneys were formed by out-of-equilibrium calcite precipitation from a predominantly hydrothermal Ca source (Fontes & Pouchan, 1975; Dekov et al., 2014). The outer layer of low-Mg calcite received Ca contributions from both hydrothermal fluids and lake waters, with a C source consisting of atmospheric CO_2 in equilibrium with alkaline lake water (Dekov et al., 2014).

The microstromatolitic crusts exhibit a combination of abiogenic and biogenic characteristics (Figs 3-12), which also seem to mirror the mixing and fluctuation of fluids. Thicker, more densely laminated layers may indicate a stronger microbial influence on precipitation, whereas thinner, isopachous acicular laminae may have formed under limited microbial influence (DeMott et al., 2021; Bisse et al., 2022). A similar configuration has been described in microdigitate lacustrine stromatolites from the Green River Formation in the USA, which formed in a similar closed-basin lacustrine system (Frantz et al., 2014). In the Green River Formation, two distinct mechanisms of carbonate formation have been identified: a fan calcitic sparite microfabric, composed of low Mg-calcite, resulting from abiogenic precipitation

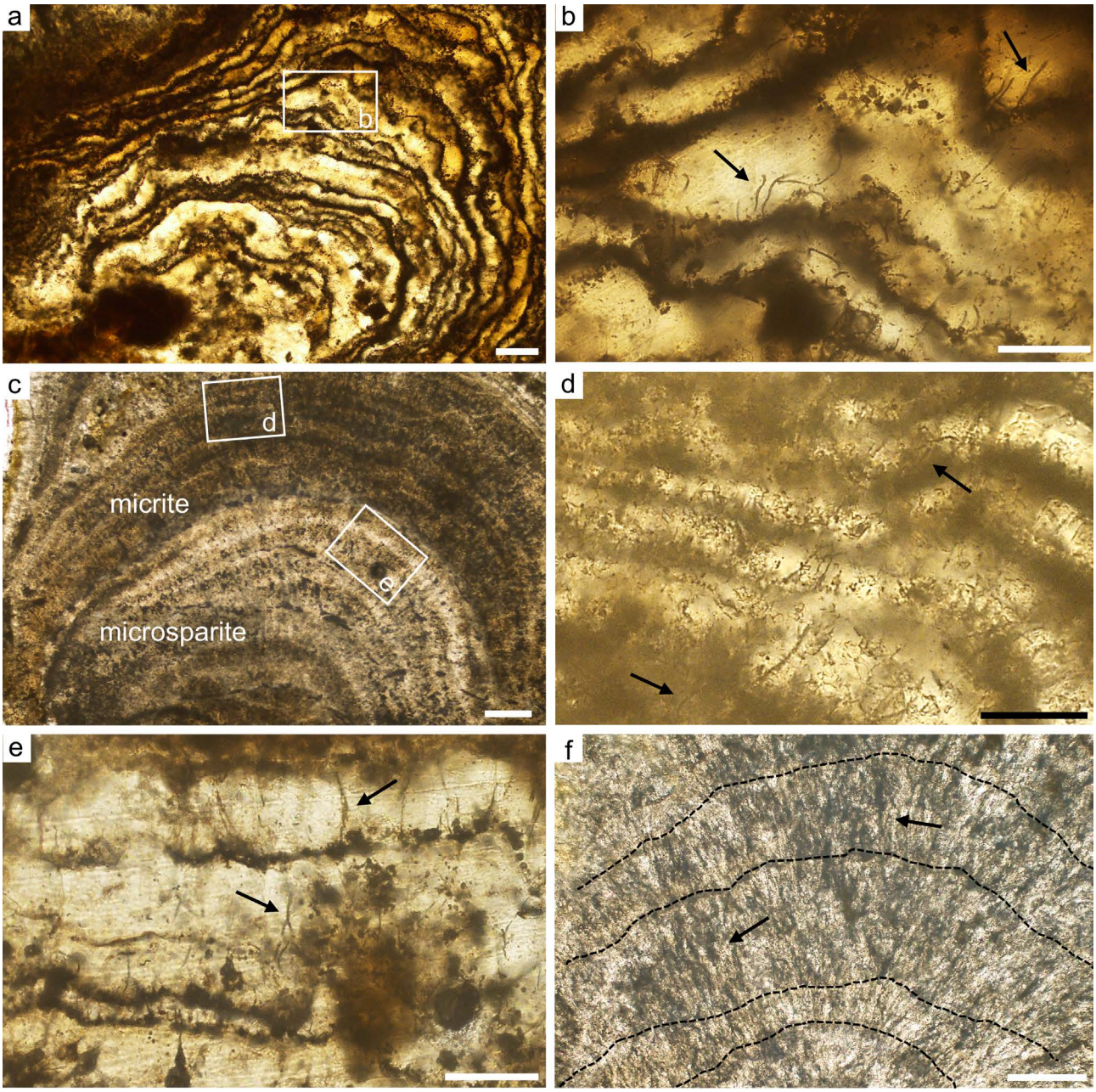

Fig. 7 - Optical photomicrographs showing laminae and filamentous structures in microcolumns. a) Wavy laminae composed of CM-reach micrite alternating with microsparite. Boxed area detailed in (b). Scale bar equals 100 µm. b) Close-up of the boxed area in (a), showing isolated filamentous structures (arrows) preserved in the microsparitic laminae. Scale bar equals 50 µm. c) Representative view of micritic and microsparite laminae preserving filamentous structures. Boxed areas detailed in (d, e). Scale bar equals 100 µm. d) Close-up of the boxed area in (c), showing isolated and clusters of filamentous structures within the micrite laminae. Scale bar equals 50 µm. e) Close-up of the boxed area in (c), showing rare and isolated filamentous structures within the microsparite laminae. Scale bar equals 50 µm. f) Filamentous aggregates forming palisade-like textures within the laminae (dashed lines). Scale bar equals 50 µm.

from lake water, and a micrite microfabric, composed of dolomite and/or calcite, resulting from microbially mediated precipitation, grain trapping and binding. Figure 10 shows a similarly striking difference between the laminae of micrite and microsparite that make up the microcolumns of the Lake Abhe microstromatolitic crusts. EDS spectra, however, detect a slight increase in Mg content in the microsparite relative to the micrite. In the Green River Formation, Frantz et al. (2014) established a direct relationship between changes in the characteristics of laminations and variations in lake level, temperature and salinity, which in turn can influence microbial development and the ability of the ecosystem to generate laminae with different fabrics. A similarly direct relationship between climate change and lake level was also detected in the lacustrine carbonate deposits of Lake Van, Turkey (Yeşilova et al., 2019).

The textural and morphological variations observed in microstromatolitic crusts at Lake Abhe can be attributed to several growth mechanisms. Internal lamination is the result of calcite precipitation mediated by cyanobacteria, whereas calcite accretion occurs through the trapping and

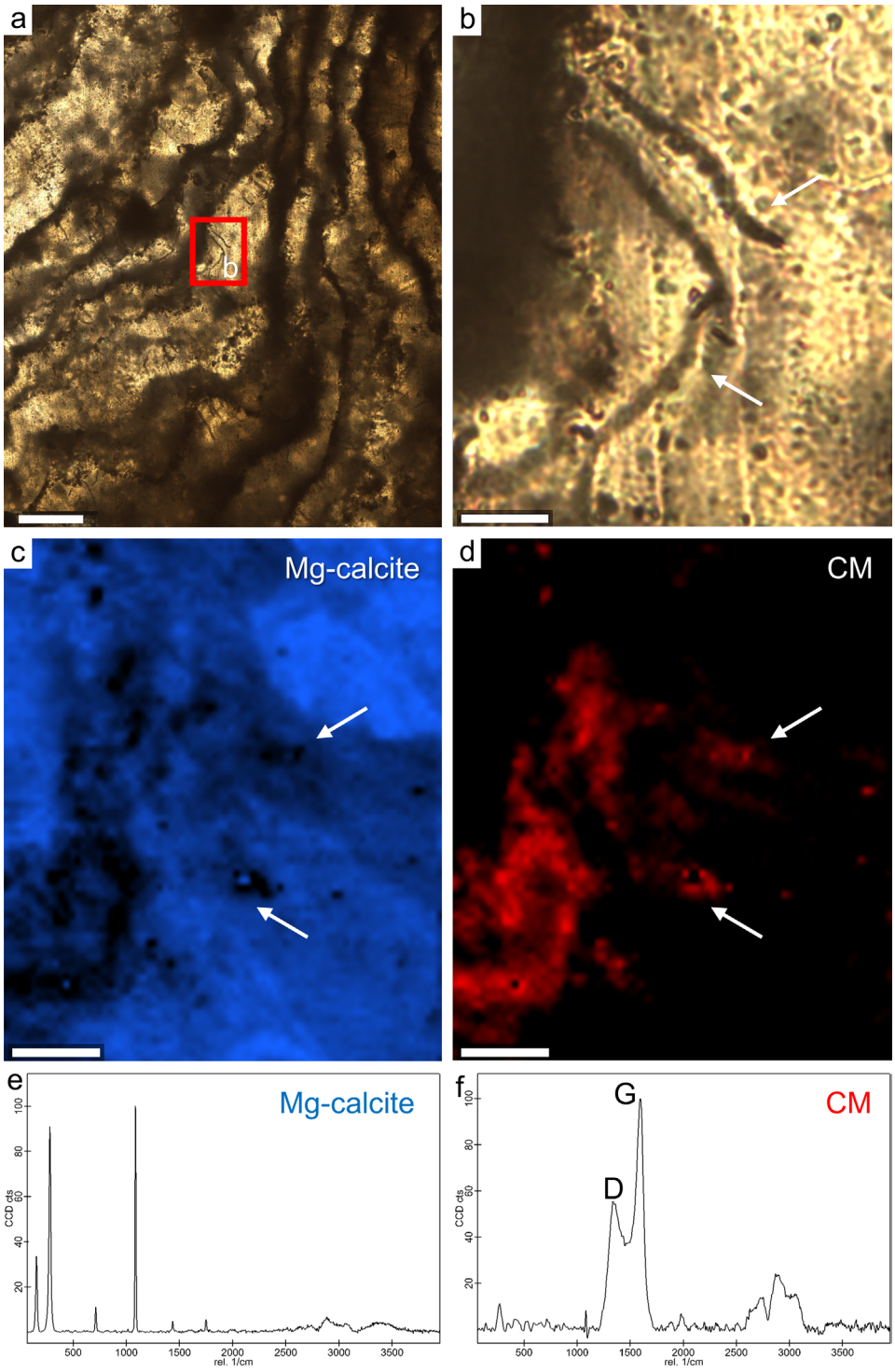

Fig. 8 - Optical photomicrographs and 2D Raman spectral maps of wavy laminae and associated filamentous structures in the microcolumnar facies. a) Optical photomicrograph showing wavy laminae (part of a microcolumn) including filamentous structures. Boxed area detailed in (b). Scale bar equals 100 µm. b) High-magnification image of the boxed area in (a) showing details of filamentous structures (arrowed). Scale bar equals 8 µm. c-f) Raman characterisation of the area imaged in (b): (c, e) show the distribution and spectral signature of Mg-calcite; (d, f) show the distribution and spectral signature of CM (arrowed). Scale bars equal 8 µm.

binding of particles, resulting in inorganic accumulation (Castro-Contreras et al., 2014). Carbonate precipitation mechanisms also seem to depend on lake currents. Micrite lamination is favoured by calm water conditions in which no sediment is deposited on the surface of the microstromatolitic crusts. Thus, calcite may precipitate from supersaturated waters, producing laminations as bacteria periodically migrate upward (Castro-Contreras et al., 2014). In hotter and drier climates, or under high evaporation conditions, alkalinity increases and the microbial community proliferates, inducing greater precipitation of laminated carbonate with preservation

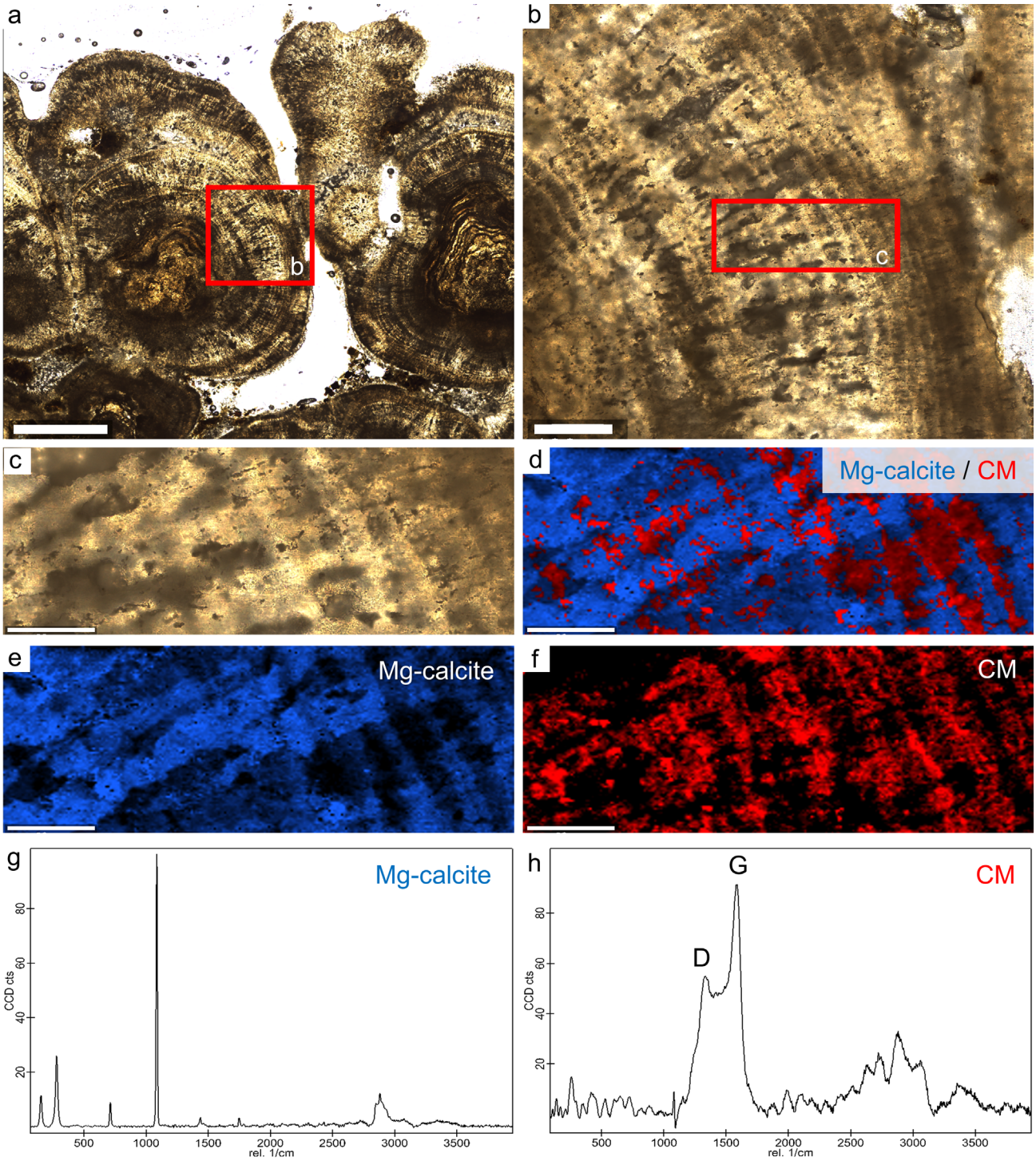

Fig. 9 - Optical photomicrographs and Raman characterisation of laminae in the crystalline fabric. a) Optical photomicrograph showing an overview of the fabrics and their association with carbonate-coated grains. Red box indicates region in (b). Scale bar equals 900 µm. b) Detail of the red box in (a), showing the flat crystalline laminae. Red box indicates the region of interest for Raman mapping. Scale bar equals 150 µm. c) Selected region of interest for Raman mapping across several laminae. d) Multiphase map showing the contrast between Mg-calcite (blue) and CM (red) in alternating layers. e, g) Raman map and spectral signature of Mg-calcite. f, h) Raman map and spectral signature of CM. Scale bars equal 60 µm.

of filaments (Muller et al., 2022). A further mechanism, detected in microbialites from the hydrothermal systems La Salsa, Bolivia (Bougeault et al., 2019), may also have occurred at Lake Abhe, whereby carbonate mineralisation may occur within the capillary waters of microbial mats at the microbial mat-air interface, where evaporation induces CO_2 degassing. CO_2 degassing through evaporation reduces the concentration of dissolved inorganic carbon within microbial mats sufficiently for the photosynthetic activity of cyanobacteria to induce a significant increase in calcite supersaturation and precipitation (Muller et al., 2022).

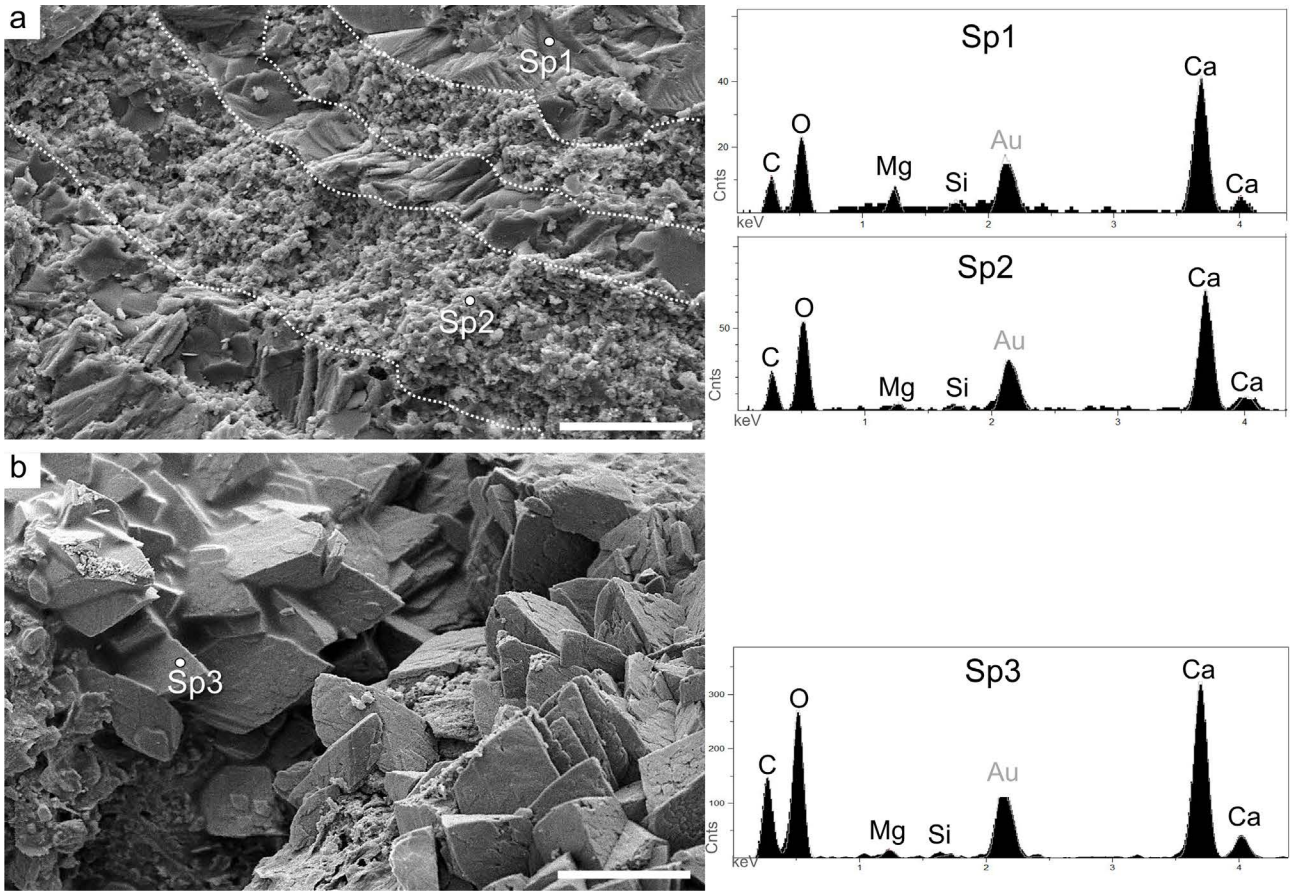

Fig. 10 - SEM and EDX characterisation of microfabrics of the microstromatolitic crusts. a) Micrograph showing laminae composed of granular micrite and microsparite calcite; EDX spectra show similar elemental compositions of predominantly Mg-calcite, with a slight variation in MgO%, and very low Si content. Scale bar equals 20 µm. b) Micrograph showing rhombohedral calcite crystals from the calcite core; EDX spectrum again indicates Mg-calcite. Scale bar equals 100 µm. In all spectra, the Au peak corresponds to the gold used for coating the samples.

The fabrics of Lake Abhe microstromatolitic crusts (Figs 4-6), such as the microcolumns and the porous calcite with a sugary texture, are comparable with those observed in microbialitic crusts from the alkaline crater lake Alchichica, Mexico (e.g., Kazmierczak et al., 2011). In Lake Alchichica, the porous cores are composed of hydromagnesite precipitated due to the rapid diagenetic replacement of primary aragonite in the living cyanobacterial biofilm. In contrast, the calcitic cores observed at Lake Abhe (Figs 4, 6c) showed no evidence of CM (Figs 5a, 6c). The euhedral and translucent Mg-calcite crystals of the core (Fig. 6c) suggest abiogenic calcite precipitation (Dupraz et al., 2009). Dekov et al. (2021), based on a comparative study of microstromatolitic crusts from Lake Abhe with similar structures from Lake Asal (Ethiopia), proposed that the calcite core (Fig. 3a) corresponds to the hot spring vents at the bases of the chimneys and fumaroles of Lake Abhe. Dendritic calcites similar to those observed in Lake Abhe seem to typify spring-associated carbonates in both subaerial and sub-lacustrine environments (Jones, 2017). Sub-lacustrine formation suggests that the inactive vents formed during periods of higher lake levels than today, and that different layers of Lake Abhe microstromatolitic crusts correspond to lake level fluctuations and regional temperature changes recorded since the Late Pleistocene and throughout of the Holocene in this region (Gasse & Street, 1978; Dekov et al., 2014; DeMott et al., 2021).

Microbe-sediment interactions

The Lake Abhe microstromatolitic crusts are dominated by authigenic carbonate with rare detrital minerals trapped within their microstructures. EDX spectra reveal trace elements, such as Mg, Al, Si, Cl, Na and K (Fig. 11) associated with fossilised carbon-rich amorphous structures, probably originating from dissolved salts and authigenic phyllosilicates, which are common in such environments (Casanova, 1994) and are not related to detrital minerals. The rarity of detrital grains suggests that microstromatolite growth occurred solely through calcite precipitation. Several factors can influence the precipitation of authigenic calcite in lake systems.

Photosynthetic absorption of CO_2 can locally increase pH and carbonate anion (CO_3^{2-}) concentration, increasing alkalinity and the activity of the Mg^{2+} and CO_3^{2-} ions, which co-precipitate with dissolved Ca^{2+} to form Mg-enriched calcite phases, mainly as microcrystalline cements (Dupraz et al., 2009; Petrash et al., 2012). As primary producers migrate up and away from the lithified substrate, the composition of water in the spaces between the detached photosynthetic biofilm and the microstromatolitic crust surface becomes temporarily controlled by microbial

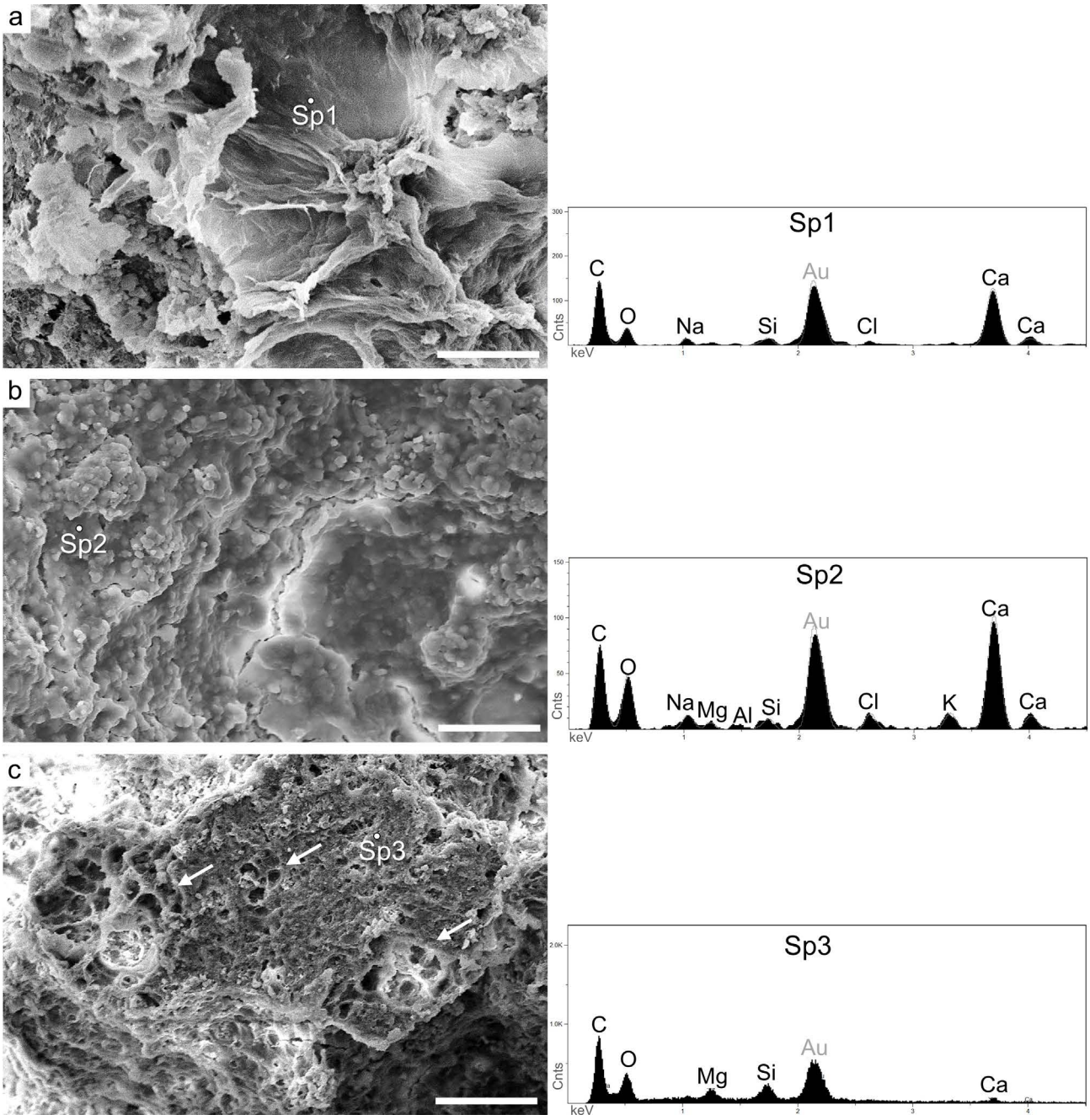

Fig. 11 - SEM micrographs and EDX spectra showing diverse carbon-rich amorphous structures derived from microbial communities in Lake Abhe microstromatolitic crusts. a) Mucus-like carbon-rich material in the matrix. Scale bar equals 10 µm. b) Carbon-rich amorphous structures associated with microgranular texture. Scale bar equals 20 µm. c) Carbon-rich amorphous structure exhibiting an alveolar network (white arrows). Scale bar equals 50 µm. In all spectra, the Au peak corresponds to the gold used for coating the samples.

metabolic activity. This activity induces physicochemical conditions that promote the rapid growth of carbonate and subsequent cementation, favouring the development of mesoscale biofilms (Dupraz & Visscher, 2005; Riding, 2006; Westall et al., 2011). This mode of carbonate precipitation is consistent with the formation of filamentous casts within a cyanobacterial sheath (Petrash et al., 2012).

The filamentous structures preserved in the Lake Abhe microstromatolitic crusts are interpreted as cyanobacterial sheaths (Figs 7-8) due to their unbranched filamentous morphology, nearly straight or flexuous morphology, and uniform diameters (Schopf, 2012; Cellamare et al., 2018), reaching up to 2.85 µm along the entire length. Many cyanobacteria are able to form mucilaginous sheaths, a distinct type of extracellular carbohydrate composed of a network of polysaccharide fibrils oriented variably relative to the cell surface (Hoiczyk, 1998; Cellamare et al., 2018). Among the morphological components of cyanobacteria, their extracellular sheath and envelopes, initially composed largely of carbohydrates and relatively resistant to degradation, are most frequently preserved in the fossil record (Schopf, 2012).

Fossilised sheaths are predominantly vertically oriented relative to the lamination of the columnar fabric

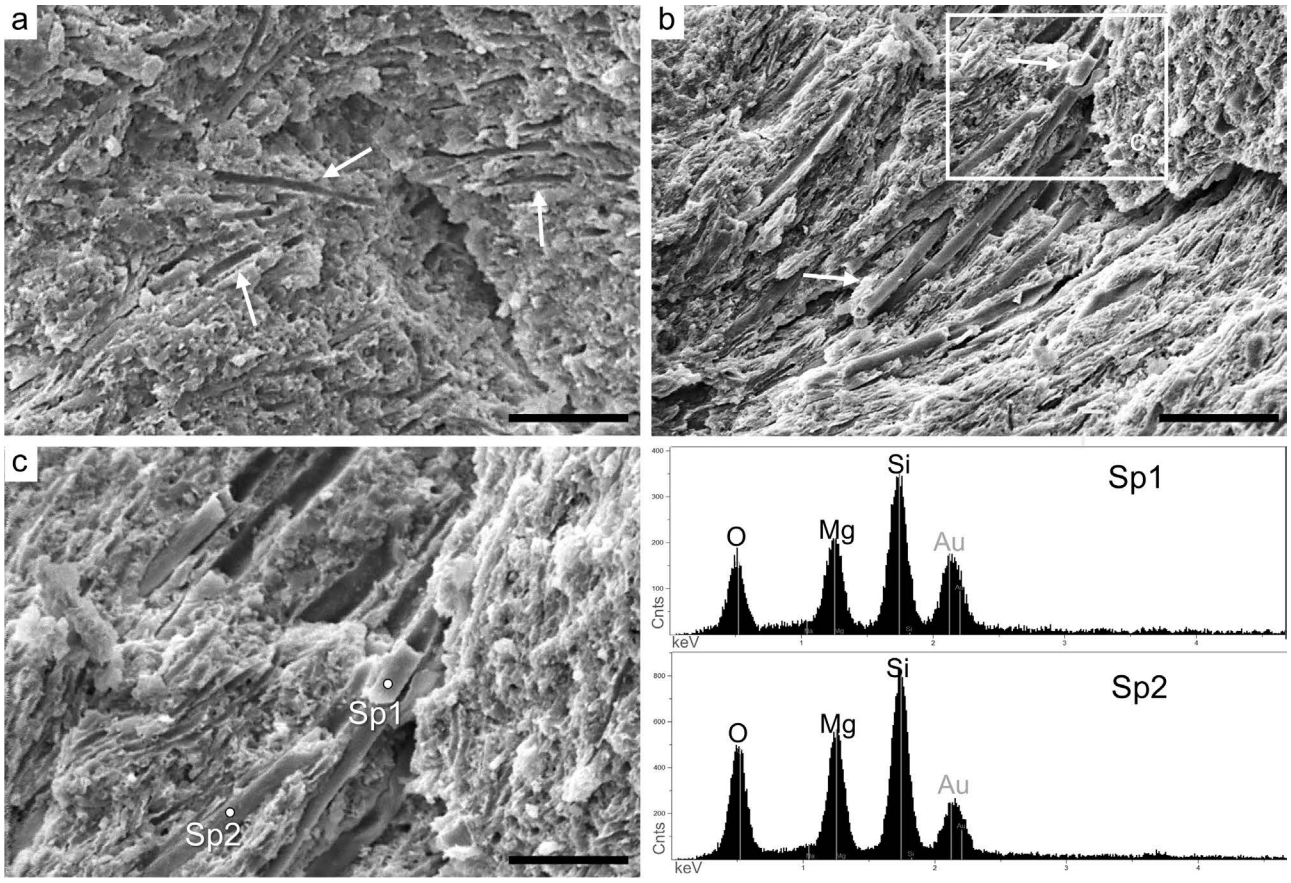

Fig. 12 - SEM micrographs showing filamentous structures. a) Filamentous empty molds (arrows) preserved in a micrite matrix. Scale bar equals 20 µm. b) Cluster of closely packed filamentous structures forming a palisade-like texture. Boxed area detailed in (c). Scale bar equals 50 µm. c) Higher magnification micrograph and EDX spectra showing molds of filaments filled with an Mg-silicate phase. Scale bar equals 20 µm. In all spectra, the Au peak corresponds to the gold used for coating the samples.

(Fig. 7), suggesting that they reflect the life position of the microbes (Berelson et al., 2011). This spatial configuration is most consistent with photosynthetic growth (Noffke & Awramik, 2013; Hickman-Lewis et al., 2019) and in some instances forms a palisade texture (Fig. 7c-f) (e.g., Franchi & Frisia, 2020). The biogenic palisade texture indicates more stable physicochemical conditions; it is associated with the growth of filamentous and sheathed cyanobacteria, forming a predominantly phototrophic ecosystem, given the shallow depositional depths (Campbell et al., 2015; Álvaro et al., 2021; Hickman-Lewis et al., 2023). Calcification of cyanobacteria appears to result from alkalinity gradients within mucilaginous sheaths, associated with photosynthetic absorption of CO_2 and/or absorption of HCO_3, which increases alkalinity (Riding, 2000).

Although stromatolite-forming ecosystems are comprised of diverse phyla, cyanobacteria play a major role in the lithification process through oxygenic photosynthesis and producing copious quantities of extracellular polymeric substances (EPS) (Dupraz et al., 2009; Nguyen et al., 2022). The carbon-rich amorphous structures observed at Lake Abhe are interpreted as EPS secreted by cyanobacteria (Figs 8-9, 11). EPS plays a central role in the formation of microbial carbonates, accumulating outside cells to form a protective, adhesive matrix that anchors microbes to substrates and provides physical and chemical protection for the biofilm community (Nguyen et al., 2022).

The process of permineralisation within stromatolites occurs due to the encrustation of cyanobacterial filaments and micritisation associated with the decomposition of the extracellular organic matrix (Dupraz et al., 2009). The presence of EPS creates nucleation sites for mineral precipitation, both absorbing essential elements used by cyanobacteria (Dupraz et al., 2009) and chelating metals that may pose toxic stresses to organisms (Hickman-Lewis et al., 2019).

Microbial preservation in Lake Abhe microstromatolitic crusts

In the Lake Abhe samples, the presence of different EPS networks may indicate the influence of varying environmental conditions on EPS degradation and carbonate precipitation (Arp et al., 2003; Calça et al., 2016). In an experiment using freshwater biofilms, Pedley (2014) found a granular EPS network similar to that described in this study (Fig. 11b) and suggested that this EPS texture, formed by amorphous calcium carbonate nanospheres, represents the initial phase of precipitation of carbonate within a biofilm. The subsequent coalescence of nanospheres and progressive occlusion of EPS resulted in the development of multilayered nanosphere aggregates, which neomorphically mature into well-

ordered microsparite crystal fabrics (Manzo et al., 2012; Pedley, 2014).

Granular EPS in the microstromatolitic crusts of Lake Abhe exhibits an elemental trace composition of Al, Si, Na, Mg, Cl and K (Fig. 11b), suggesting the presence of aluminous phyllosilicates, such as kaolinite. Fiore et al. (2011) experimentally proposed that the formation of Al-rich silicate phases occurs through the precipitation of an aluminosilicate gel within the EPS; and that the crystallisation of kaolinite takes place as a consequence of changes in the microenvironment induced by metabolic activity, suggesting localised syndepositional mineralisation and carbonate-silica interplay within granular EPS in the Lake Abhe microstromatolitic crusts.

In addition to the granular EPS, an alveolar network of EPS was also observed (Fig. 11c). Dupraz et al. (2004) proposed that alveolar EPS may form due to the initial precipitation of Mg-rich calcite and the activity of sulphate-reducing bacteria. This occurs because the acidic macromolecules in microbial biofilms can reorganise into a structured pattern to provide nucleation sites for carbonate, potentially influenced by decaying EPS, as suggested by Trichet et al. (2001) and Calça et al. (2016).

The alveolar EPS in Lake Abhe microstromatolitic crusts contains Mg, Si and O (Fig. 11c), interpreted as Mg-silicate. Burne et al. (2014) proposed that Mg-silicate forms within and around cyanobacterial sheaths and in the EPS alveolar network, driven by high silica activity and reduced C and Ca in the EPS due to biological processes. In Lake Abhe, cyanobacterial sheath molds filled with Mg- and Si-rich material (Fig. 12b-c) support this model, indicating the potential accumulation of Mg-silicate minerals as syndepositional clay within laminated sediments (DeMott et al., 2021).

The authigenic microbial precipitation of Mg-bearing phyllosilicates, such as stevensite, has been reported in alkaline lakes as a syngenetic phase often associated with carbonates. In Lake Clifton, Australia, Burne et al. (2014) described Mg-Si phases forming within and around cyanobacterial sheaths, similar to the filled molds in Lake Abhe samples (Fig. 12b-c). Burne et al. (2014) demonstrated that stevensite permineralised the walls of the filamentous sheaths and nucleated on the surface of the microbial filaments in thrombolites. This led to massive stevensite formation, followed by carbonate replacement of cyanobacterial remnants. Carbonates initially form radiating rhombic microcrystals that coalesce into dense aggregates, obscuring the original fabric, as demonstrated experimentally by Manzo et al. (2012).

Mg-bearing silicates play a crucial role in preserving filaments and their molds, as well as EPS, in volcanically influenced alkaline lacustrine systems (e.g., Mologni et al., 2021). Lincoln et al. (2022) studied Mg-silicates and aragonite in Great Salt Lake ooid cortices, concluding that microbial mediation is likely responsible for their formation. Raman analysis of Lake Abhe microstromatolitic crusts found a high concentration of presumably microbially derived CM in the concentric laminations of the carbonate-coated grains, supporting a similarly biomediated mechanism of formation. Pace et al. (2016) also documented amorphous Mg-silicates in modern microbialites from the Great Salt Lake, suggesting microbially mediated precipitation due to localised pH increases. The Mg-Si phase, a precursor to stevensite in the Great Salt Lake, was precipitated within the organic matrix by incorporating Mg^{2+} and SiO_2 from the lake water. The microbial metabolism lowers the kinetic barrier for Mg-Si phase nucleation and induces the precipitation of this poorly crystalline phase. According to Tosca et al. (2011), the formation of poorly crystalline Mg-silicate indicates that the lake waters were highly alkaline (pH > 8.7). Lake Abhe, characterised by pH 9.9 and a high content of dissolved SiO_2 (~ 416 mg/L^{-1}; Gasse, 1977), presents an ideal environment for Mg-silicate formation. In the chimney samples, the absence of significant diagenetic alteration features, such as dissolution, dolomitisation and cementation associated with pore occlusion, also suggests that the presence of magnesium-bearing clay minerals is neither a product of secondary minerals filling the pores, nor a result of early calcite alteration, consistent with the findings of DeMott et al. (2021).

CONCLUSIONS

Microstromatolitic structures encrusting carbonate chimneys and basaltic bedrock at Lake Abhe, Republic of Djibouti, are dominated by Mg-calcite laminated fabrics. Their formation is clearly influenced by the presence of cyanobacteria-dominated communities that thrived in this extreme alkaline lake. Microcolumnar stromatolitic fabrics are dominated by filamentous structures; however, filamentous structures were also found to be preserved in crystalline fabrics and in association with carbonate-coated grains.

Cyanobacterial sheaths and EPS are the most abundant microbial components responsible for the formation of microstromatolitic crusts. Cyanobacterial sheath molds are primarily preserved in a palisade-like texture, suggesting preservation in life position, and strongly supporting the photosynthetic metabolic dominance of the ecosystem. Sheath molds are filled with Mg-rich silicate materials, suggesting that syn-depositional clay accumulation may have played a major role in their preservation. EPS also played a crucial role in microbial carbonate formation and preservation, providing a protective and adhesive matrix that aided in carbonate precipitation and fossilisation processes.

The Lake Abhe microstromatolitic crusts demonstrate good fossilisation potential. The carbonaceous composition of their biogenic components appears to have been preserved in association with specific combinations of Mg-bearing silicate and carbonate phases. Such depositional and diagenetic conditions may be particularly beneficial for the formation of organic-mineral associations that promote the preservation of filamentous microfossils in highly alkaline, basalt-hosted lacustrine environments.

ACKNOWLEDGEMENTS

The samples were collected with the authorization of CERD (Centre d'Étude et de Recherche de Djibouti) and with the agreement of the General Manager, Dr. Jalludin Mohamed. The authors gratefully acknowledge Giorgio Gasparotto, Fabio Gamberini, Irene Albino, Davide Cavalletti, Lucas Jacquier and Oleksandra Shcherbyna for their assistance in preparing and analysing samples.

We thank Brahim Abounacer for field assistance. BC and RB acknowledge grants RFO2018-UNIBO and RFO2019-UNIBO. KHL acknowledges support from the UK Space Agency (Aurora Research Fellowship, grant nos. ST/V00560X/1 and ST/Z000491/1). VACD and KHL acknowledge funding from the Europlanet 2024 RI Expert Exchange Programme (Grant agreement no. 871149).

REFERENCES

Abbate E., Passerini P. & Zan L. (1995). Strike-slip faults in a rift area: a transect in the Afar Triangle, East Africa. *Tectonophysics*, 241: 67-97.

Álvaro J.J., Sánchez-Román M., Nierop K.G. & Peterse F. (2021). Multiscale microbial preservation and biogeochemical signals in a modern hot-spring siliceous sinter rich in CO_2 emissions, Krýsuvík geothermal field, Iceland. *Minerals*, 11: 263.

Arp G., Reimer A. & Reitner J. (2003). Microbialite formation in seawater of increased alkalinity, Satonda Crater Lake, Indonesia. *Journal of Sedimentary Research*, 73: 105-127.

Awaleh M.O., Hoch F.B., Boschetti T., Soubaneh Y.D., Egueh N.M., Elmi S.A., Mohamed J. & Khaireh M.A. (2015). The geothermal resources of the Republic of Djibouti—II: Geochemical study of the Lake Abhe geothermal field. *Journal of Geochemical Exploration*, 159: 129-147.

Berelson W.M., Corsetti F.A., Pepe-Ranney C., Hammond D.E., Beaumont W. & Spear J.R. (2011). Hot spring siliceous stromatolites from Yellowstone National Park: assessing growth rate and laminae formation. *Geobiology*, 9: 411-424.

Bisse S.B., Ekoko B.E., Gerber J., Ekomane E. & Franchi F. (2022). Influence of biotic vs abiotic processes on the genesis of non-marine carbonates along the Cameroon Volcanic Line (Cameroon) and palaeofluid provenance. *The Depositional Record*, 8: 102-126.

Bosak T., Knoll A.H. & Petroff A.P. (2013). The meaning of stromatolites. *Annual Review of Earth and Planetary Sciences*, 41: 21-44.

Boschetti T., Awaleh M. & Barbieri M. (2018). Waters from the Djiboutian Afar: A Review of Strontium Isotopic Composition and a Comparison with Ethiopian Waters and Red Sea Brines. *Water*, 10: 1700.

Bougeault C., Vennin E., Durlet C., Muller E., Mercuzot M., Chavez M., Gérard E., Ader M., Virgone A. & Gaucher E.C. (2019). Biotic-abiotic influences on modern Ca–Si-rich hydrothermal spring mounds of the Pastos Grandes volcanic caldera (Bolivia). *Minerals*, 9: 380.

Burne R.V. & Moore L.S. (1987). Microbialites: organosedimentary deposits of benthic microbial communities. *Palaios*, 1: 241-254.

Burne R.V., Moore L.S., Christy A.G., Troitzsch U., King P.L., Carnerup A.M. & Hamilton P.J. (2014). Stevensite in the modern thrombolites of Lake Clifton, Western Australia: a missing link in microbialite mineralization?. *Geology*, 42: 575-578.

Çağatay M.N., Damci E., Bayon G. & Sari M. (2024). Microbialites on the northern shelf of Lake Van, eastern Türkiye: Morphology, texture, stable isotope geochemistry and age. *Sedimentology*, 71: 850-870.

Calça C.P., Fairchild T.R., Cavalazzi B., Hachiro, J., Petri S., Huila M.F.G., Toma H.E. & Araki K. (2016). Dolomitized cells within chert of the Permian Assistência Formation, Paraná Basin, Brazil. *Sedimentary Geology*, 335: 120-135.

Caminiti A.M. (2000). Le fossé d'Asal et le Lac Abhé: deux sites géologiques exceptionnels en République de Djibouti. 132 pp. Edition Couleur Locale, Djibouti.

Campbell K.A., Lynne B.Y., Handley K.M., Jordan S., Farmer J.D., Guido D.M., Foucher F., Turner S. & Perry R.S. (2015). Tracing biosignature preservation of geothermally silicified microbial textures into the geological record. *Astrobiology*, 15: 858-882.

Casanova J. (1994). Stromatolites from the East African Rift: A synopsis. *In* Bertrand-Sarfati J. & Monty C. (eds), Phanerozoic Stromatolites II. Springer, Dordrecht: 193-226.

Castro-Contreras S.I., Gingras M.K., Pecoits E., Aubet N.R., Petrash D., Castro-Contreras S.M., Dick G., Planavsky N. & Konhauser K.O. (2014). Textural and geochemical features of freshwater microbialites from Laguna Bacalar, Quintana Roo, Mexico. *Palaios*, 29: 192-209.

Cavalazzi B, Barbieri R., Cady S.L., George A.D., Gennaro S., Westall F., Lui A., Canteri R., Rossi A.P., Ori G.G. & Taj-Eddine K. (2012). Iron-framboids in the hydrocarbon-related Middle Devonian Hollard Mound of the Anti-Atlas mountain range in Morocco: Evidence of potential microbial biosignatures. *Sedimentary Geology*, 263-264: 183-193.

Cavalazzi B., Barbieri R., Gómez F., Capaccioni B., Olsson-Francis K., Pondrelli M., Rossi A.P., Hickman-Lewis K., Agangi A., Gasparotto G., Glamoclija M., Ori G.G., Rodriguez N. & Hagod M. (2019). The Dallol geothermal area, Northern Afar (Ethiopia)—An exceptional planetary field analog on Earth. *Astrobiology*, 19: 553-578.

Cellamare M., Duval C., Drelin Y., Djediat C., Touibi N., Agogué H., Leboulanger C., Ader M. & Bernard C. (2018). Characterization of phototrophic microorganisms and description of new cyanobacteria isolated from the saline-alkaline crater-lake Dziani Dzaha (Mayotte, Indian Ocean). *FEMS Microbiology Ecology*, 94: 108.

Coman C., Chiriac C.M., Robeson M.S., Ionescu C., Dragos N., Barbu-Tudoran L., Andrei A.Ş., Banciu H.L., Sicora C. & Podar M. (2015). Structure, mineralogy, and microbial diversity of geothermal spring microbialites associated with a deep oil drilling in Romania. *Frontiers in Microbiology*, 6: 253.

Corti G. (2009). Continental rift evolution: from rift initiation to incipient break-up in the Main Ethiopian Rift, East Africa. *Earth-Science Reviews*, 96: 1-53.

Dekov V.M., Egueh N.M., Kamenov G.D., Bayon G., Lalonde S.V., Schmidt M., Liebetrau V., Munnik F., Fouquet Y., Tanimizu M. & Awaleh M.O. (2014). Hydrothermal carbonate chimneys from a continental rift (Afar Rift): Mineralogy, geochemistry, and mode of formation. *Chemical Geology*, 387: 87-100.

Dekov V.M., Gueguen B., Yamanaka T., Moussa N., Okumura T., Bayon G., Liebetrau V., Yoshimura T., Kamenov G., Araoka D. & Makita H. (2021). When a mid-ocean ridge encroaches a continent: Seafloor-type hydrothermal activity in Lake Asal (Afar Rift). *Chemical Geology*, 568: 120126.

Demange J., Di Paola G.M., Lavigne J.J., Lopoukhine M. & Stieltjes L. (1971). Etude géothermique du Territoire Français des Afars et des Issas. *Rapport de Recherches Géologiques et Minières*, 71: 262.

DeMott L.M., Scholz C.A. & Awaleh M.O. (2021). Lacustrine carbonate towers of Lake Abhe, Djibouti: Interplay of hydrologic and microbial processes. *Sedimentary Geology*, 424: 105983.

Dupraz C. & Visscher P.T. (2005). Microbial lithification in marine stromatolites and hypersaline mats. *Trends in microbiology*, 13: 429-438.

Dupraz C., Visscher P.T., Baumgartner L.K. & Reid R.P. (2004). Microbe–mineral interactions: early carbonate precipitation in a hypersaline lake (Eleuthera Island, Bahamas). *Sedimentology*, 51: 745-765.

Dupraz C., Reid R.P., Braissant O., Decho A.W., Norman R.S. & Visscher P.T. (2009). Processes of carbonate precipitation in modern microbial mats. *Earth-Science Reviews*, 96: 141-162.

Farías M.E., Rascovan N., Toneatti D.M., Albarracín V.H., Flores M.R., Poiré D.G., Collavino M.M., Aguilar O.M., Vazquez M.P. & Polerecky L. (2013). The discovery of stromatolites developing at 3570 m above sea level in a high-altitude volcanic lake Socompa, Argentinean Andes. *PLOS ONE*, 8: e53497.

Fiore S., Dumontet S., Huertas F.J. & Pasquale V. (2011). Bacteria-induced crystallization of kaolinite. *Applied Clay Science*, 53: 5566-5571.

Fontes J.C. & Pouchan P. (1975). Les cheminées du Lac Abbé (TFAI): Stations hydroclimatiques de l'Holocéne. *Comptes Rendus de l'Académie des Sciences Paris*, 280: 383-385.

Foster J.S., Green S.J., Ahrendt S.R., Golubic S., Reid R.P., Hetherington K.L. & Bebout L. (2009). Molecular and morphological characterization of cyanobacterial diversity in the stromatolites of Highborne Cay, Bahamas. *The ISME Journal - Multidisciplinary Journal of Microbial Ecology,* 3: 573-587.

Franchi F. & Frisia S. (2020). Crystallization pathways in the Great Artesian Basin (Australia) spring mound carbonates: implications for life signatures on Earth and beyond. *Sedimentology*, 67: 2561-2595.

Frantz C.M., Petryshyn V.A., Marenco P.J., Tripati A., Berelson W.M. & Corsetti F.A. (2014). Dramatic local environmental change during the Early Eocene Climatic Optimum detected using high resolution chemical analyses of Green River Formation stromatolites. *Palaeogeography, Palaeoclimatology, Palaeoecology*, 405: 1-15.

Frezzotti M.L., Tecce F. & Casagli A. (2011). Raman spectroscopy for fluid inclusion analysis. *Journal of Geochemical Exploration*, 112: 1-20.

Gasse F. & Fontes J.C. (1989). Palaeoenvironments and palaeohydrology of a tropical closed lake (Lake Asal, Djibouti) since 10,000 yr BP. *Palaeogeography, Palaeoclimatology, Palaeoecology*, 69: 67-102.

Gasse E. & Street F.A. (1978). Late Quaternary lake-level fluctuations and environments of the northern Rift Valley and Afar region (Ethiopia and Djibouti). *Palaeogeography, Palaeoclimatology, Palaeoecology*, 24: 279-325.

Gasse F. (1977). Evolution of Lake Abhé (Ethiopia and TFAI), from 70,000 bp. *Nature*, 265: 42-45.

Gasse F. (2000). Hydrological changes in the African tropics since the Last Glacial Maximum. *Quaternary Science Reviews*, 19: 189-211.

Grotzinger J.P. & Knoll A.H. (1999). Stromatolites in Precambrian carbonates: evolutionary mileposts or environmental dipsticks?. *Annual Review of Earth and Planetary Sciences*, 27: 313-358.

Gutherz X., Lesur J., Cauliez J., Charpentier V., Diaz A., Ismaël M.O., Pène J.M., Sordoillet D. & Zazzo A. (2015). New insights on the first Neolithic societies in the Horn of Africa: The site of Wakrita, Djibouti. *Journal of Field Archaeology*, 40: 55-68.

Hickman-Lewis K., Gautret P., Arbaret L., Sorieul S., De Wit R., Foucher F., Cavalazzi B. & Westall F. (2019). Mechanistic morphogenesis of organo-sedimentary structures growing under geochemically stressed conditions: keystone to proving the biogenicity of some Archaean stromatolites? *Geosciences*, 9: 359.

Hickman-Lewis K., Cavalazzi B., Giannoukos K., d'Amico L., Vrbaski S., Saccomano G., Dreossi D., Tromba G., Foucher F., Brownscombe W., Smith C.L. & Westall F. (2023). Advanced two-and three-dimensional insights into Earth's oldest stromatolites (ca. 3.5 Ga): Prospects for the search for life on Mars. *Geology*, 51: 33-38.

Hoiczyk E. (1998). Structural and biochemical analysis of the sheath of *Phormidium uncinatum*. *Journal of Bacteriology*, 180: 3923-3932.

Jahnert R.J. & Collins L.B. (2012). Characteristics, distribution and morphogenesis of subtidal microbial systems in Shark Bay, Australia. *Marine Geology*, 303: 115-136.

Jones B. (2017). Review of aragonite and calcite crystal morphogenesis in thermal spring systems. *Sedimentary Geology*, 354: 9-23.

Kaźmierczak J., Kempe S., Kremer B., López-García P., Moreira D. & Tavera R. (2011). Hydrochemistry and microbialites of the alkaline crater lake Alchichica, Mexico. *Facies*, 57: 543-570.

Laetsch T.A. & Downs R.T. (2006). Software for identification and refinement of cell parameters from powder diffraction data of minerals using the RRUFF Project and American Mineralogist Crystal Structure Databases. *Program and Abstracts of the 19th General Meeting of the International Mineralogical Association in Kobe, Japan,* 2006: 08-25.

Le Gall B., Jalludin M., Maury R., Gasse F., Daoud M.A., Gutherz X., Doubre C., Caminiti A.M., Moussa N. & Rolet J. (2018). Notice de la carte géologique au 1/200000 de la République de Djibouti. 200 pp. Centre d'Étude et de Recherche de Djibouti CERD-CGGM. Djibouti.

Lincoln T.A., Webb S.M., Present T.M., Magyar J.S. & Trower E.J. (2022). Microbial activity and neomorphism influence the composition and microfabric of ooids from Great Salt Lake, UT. *The Sedimentary Record*, 20: 1-10.

Manzo E., Perri E. & Tucker M.E. (2012). Carbonate deposition in a fluvial tufa system: processes and products (Corvino Valley–southern Italy). *Sedimentology*, 59: 553-577.

McCall J. (2010). Lake Bogoria, Kenya: Hot and warm springs, geysers and Holocene stromatolites. *Earth-Science Reviews*, 103: 71-79.

Mologni C., Bruxelles L., Schuster M., Davtian G., Ménard C., Orange F., Doubre C., Cauliez J., Taezaz H.B., Revel M. & Khalidi L. (2021). Holocene East African monsoonal variations recorded in wave-dominated clastic paleo-shorelines of Lake Abhe, Central Afar region (Ethiopia & Djibouti). *Geomorphology*, 391: 107896.

Muller E., Ader M., Aloisi G., Bougeault C., Durlet C., Vennin E., Benzerara K., Gaucher E.C., Virgone A., Chavez M., Souquet P. & Gérard E. (2022). Successive Modes of Carbonate Precipitation in Microbialites along the Hydrothermal Spring of La Salsa in Laguna Pastos Grandes (Bolivian Altiplano). *Geosciences*, 12: 88.

Nguyen S.T., Vardeh D.P., Nelson T.M., Pearson L.A., Kinsela A.S. & Neilan B.A. (2022). Bacterial community structure and metabolic potential in microbialite-forming mats from South Australian saline lakes. *Geobiology*, 20: 546-559.

Noffke N. & Awramik S.M. (2013). Stromatolites and MISS—differences between relatives. *GSA Today*, 23: 4-9.

Nutman A.P., Bennett V.C., Friend C.R., Van Kranendonk M.J. & Chivas A.R. (2016). Rapid emergence of life shown by discovery of 3,700-million-year-old microbial structures. *Nature*, 537: 535-538.

Pace A., Bourillot R., Bouton A., Vennin E., Galaup S., Bundeleva I., Patrier P., Dupraz C., Thomazo C., Sansjofre P. & Yokoyama Y. (2016). Microbial and diagenetic steps leading to the mineralisation of Great Salt Lake microbialites. *Scientific Reports*, 6: 31495.

Papineau D., Walker J.J., Mojzsis S.J. & Pace N.R. (2005). Composition and structure of microbial communities from stromatolites of Hamelin Pool in Shark Bay, Western Australia. *Applied and Environmental Microbiology*, 71: 4822-4832.

Pedley M. (2014). The morphology and function of thrombolitic calcite precipitating biofilms: A universal model derived from freshwater mesocosm experiments. *Sedimentology*, 61: 22-40.

Petrash D.A., Gingras M.K., Lalonde S.V., Orange F., Pecoits E. & Konhauser K.O. (2012). Dynamic controls on accretion and lithification of modern gypsum-dominated thrombolites, Los Roques, Venezuela. *Sedimentary Geology*, 245: 29-47.

Riding R. (2000). Microbial carbonates: the geological record of calcified bacterial-algal mats and biofilms. *Sedimentology*, 47: 179-214.

Riding R. (2011). Microbialites, stromatolites, and thrombolites. *In* Reitner J. & Thiel V. (eds), Encyclopedia of Geobiology. Springer Science, Heidelberg: 635-654.

Riding R. (2006). Cyanobacterial calcification, carbon dioxide concentrating mechanisms, and Proterozoic-Cambrian changes in atmospheric composition. *Geobiology*, 4: 299-316.

Schopf J.W. (2012). The fossil record of cyanobacteria. *In* Whitton B.A. & Potts M. (eds), Ecology of Cyanobacteria II: Their Diversity in Space and Time. Springer Science, Dordrecht: 15-36.

Tesfaye S., Harding D.J. & Kusky T.M. (2003). Early continental breakup boundary and migration of the Afar triple junction, Ethiopia. *Geological Society of America Bulletin*, 115: 1053-1067.

Tosca N.J., Macdonald F.A., Strauss J.V., Johnston D.T. & Knoll A.H. (2011). Sedimentary talc in Neoproterozoic carbonate successions. *Earth and Planetary Science Letters*, 306: 11-22.

Trichet J., Défarge C., Tribble J., Tribble G. & Sansone F. (2001). Christmas Island lagoonal lakes, models for the deposition of carbonate–evaporite–organic laminated sediments. *Sedimentary Geology*, 140: 177-189.

Valette J.N. (1975). Le lac Abhé (T.F.A.I.): étude morphologique et géochimique. *Bulletin Bureau de Recherches Géologiques et Minières, deuxième série, Section II*, 2: 143-155.

Varet J. (2018). Geology of Afar (East Africa), 336 pp. Springer International Publishing, Switzerland.

Walter B., Géraud Y., Favier A., Chibati N. & Diraison M. (2023). Hydrothermal activity of the Lake Abhe geothermal field (Djibouti): Structural controls and paths for further exploration. EGUsphere, 2023: 1-24.

Westall F., Cavalazzi B., Lemelle L., Marrocchi Y., Rouzaud J.-N., Simionovici A., Salomé M., Mostefaoui S., Andreazza C., Foucher F., Toporski J., Jauss A., Thiel V., Southam G., MacLean L., Wirick S., Hofmann A., Meibom A., Robert F. & Défarge C. (2011) Implications of in situ calcification for photosynthesis in a ~3.3Ga-old microbial biofilm from the Barberton greenstone belt, South Africa. Earth and Planetary Scienze Letters, 310: 468-479.

Yeşilova Ç., Gülyüz E., Huang C.R. & Shen C.C. (2019). Giant tufas of Lake Van record lake-level fluctuations and climatic changes in eastern Anatolia, Turkey. *Palaeogeography, Palaeoclimatology, Palaeoecology*, 533: 109226.

Zăinescu F., Van der Vegt H., Storms J., Nutz A., Bozetti G., May J.H., Cohen S., Bouchette F., May S.M. & Schuster M. (2023). The role of wind-wave related processes in redistributing river-derived terrigenous sediments in Lake Turkana: A modelling study. *Journal of Great Lakes Research*, 49: 368-386.

Manuscript submitted 9 September 2024
Revised manuscript accepted 27 October 2024
Published online 28 December 2024
Editor Silvia Danise